IEEE Access
Multidisciplinary | Rapid Review | Open Access Journal

Received November 25, 2020, accepted December 13, 2020, date of publication December 16, 2020,
date of current version December 29, 2020.

Digital Object Identifier 10.1109/ACCESS.2020.3045227

Research on Motion Mode Switching Method Based on CPG Network Reconstruction

ZHEPING YAN, HAOYU YANG, WEI ZHANG, QINGSHUO GONG, AND FANTAI LIN
College of Intelligent Systems Science and Engineering, Harbin Engineering University, Harbin 150001, China

Corresponding author: Wei Zhang (yanghaoyu@hebeu.edu.cn)

This work was supported in part by the National Natural Science Foundation of China under Grant 51679057 and Grant E1102/52071108, in part by the National Nature Science Foundation of China under Grant 51609046, and in part by the Province Science Fund for Distinguished Young Scholars under Grant J2016JQ0052.

ABSTRACT Traditional underwater robots have many shortcomings in terms of resistance to sea currents, stability and functionality. In order to improve the efficiency and quality of underwater operations, this paper proposes and designs a new underwater robot, the navigation and crawl underwater unmanned vehicle (NCUUV), it has two motion modes: swimming and crawling. In order to enable the robot to have the ability to switch motion modes, this paper designed a motion mode switching mechanism, and verified the effectiveness of the mechanism through experiments, which proved that the mechanism has good motion reliability and accuracy. In order to control NCUUV to smoothly switch the motion mode, a controller based on the central pattern generator (CPG) was developed. The upper controller reconstructs the CPG network in the middle controller according to the feedback information of the acoustic rangefinder. The CPG network in the middle controller has two configurations: a triangular fully symmetrical network and a hexagonal fully symmetrical network, and the CPG network can be freely changed between the two configurations according to the instructions of the upper controller. These two configurations control NCUUV's swimming and crawling respectively, so as to realize the smooth switching between swimming and crawling. The experimental result shows that this control mechanism of motion mode switching can enable NCUUV to stably realize motion mode switching and the switching process is smooth and reliable.

INDEX TERMS Underwater robot, swimming, crawling, motion mode switching, central pattern generator.

I. INTRODUCTION

Traditional unmanned underwater vehicles mostly use impellers and propellers to provide power. This type of propulsion has problems such as low efficiency, high noise, large disturbance to the surrounding environment, and poor concealment [1]–[3]. As people further develop the ocean, underwater operations present a wide range, large depth, long time, multi-function and other characteristics, which undoubtedly put forward higher requirements for underwater vehicles. After hundreds of millions of years of evolution, fish have huge advantages in terms of propulsion efficiency, maneuverability and concealment [4], [5]. Therefore, compared with traditional underwater vehicles, bionic fish has significant advantages in energy saving, maneuverability and concealment. It is playing an increasingly important role in underwater archaeology, water quality monitoring, underwater resource exploration, military reconnaissance and other fields.

As the focus of bionic fish research, motion control has also been greatly developed. Biologists have discovered that the movements of vertebrates and invertebrates are controlled by a neural network called a central pattern generator (CPG). CPG does not require rhythmic control or feedback input to produce rhythmic behaviors, such as walking, swimming, flying, breathing, and chewing, etc [6].

Scientists and engineers have found that CPG has strong robustness, and can be coupled with a variety of feedback, and has unparalleled advantages in coordinated motion control of multiple degrees of freedom. The motion control of the bionic fish is a typical representative of multi-DOF coordinated control, so CPG control is increasingly being applied to the motion control of the bionic fish [7]–[9]. Cafer Bal *et al.* proposed a finite state machine based on fuzzy control, which can adjust the CPG output according to different feedback information, so that the robot fish has good ability of autonomous

The associate editor coordinating the review of this manuscript and approving it for publication was Jinpeng Yu.

This work is licensed under a Creative Commons Attribution 4.0 License. For more information, see https://creativecommons.org/licenses/by/4.0/

obstacle avoidance [10]. Junzhi Yu, Wang Ming *et al.* optimized the output parameters of CPG through particle swarm optimization, improved the propulsion efficiency and speed of the robot fish, and explored the effect of CPG characteristic parameters on energy consumption during the swimming process of the robot fish [11]–[13]. Ming Wang *et al.* proposed an iterative learning method and conducted simulation experiments for the problem of robotic fish swimming trajectory tracking control, which verified the effectiveness of the trajectory tracking control method based on iterative learning [14]. JiaQuan Z *et al.* designed an adaptive fuzzy control algorithm to control the direction and speed of the robotic fish in real time, so that the robotic fish can reach the target point quickly and accurately, which effectively improves the control accuracy of the robotic fish [15]. Some scholars also used fuzzy control or fuzzy PID control to control the attack angle of the pectoral fin and the deflection angle of the caudal fin, thus realizing the diving, floating and depth control of the robotic fish [16]–[18].

Although the robotic fish has many functions such as cruising, hovering, underwater loading, like traditional underwater vehicles, it still uses the hovering method for underwater operations, so this work mode is very susceptible to ocean currents. In order to resist the effect of ocean currents, on the one hand, people continue to improve the control accuracy of underwater vehicles, on the other hand, based on the characteristics of land-footed robots, underwater-footed robots have been developed.

Because CPG control has good flexibility and robustness, it has also been widely used in footed robots and has gradually developed into a research focus. Zhu *et al.* proposed several typical gait patterns, and extended them to mixed gait, realizing the omnidirectional walking of the hexapod robot on the ground [19]. Faigl J *et al.* proposed the use of adaptive motion control to detect the contact point between the leg and the ground, and judge the contact situation between the foot and the ground by the torque of the feedback steering gear, so that the small hexapod robot can walk on the rugged terrain [20]. Daniel Gutierrez-Galan *et al.* preset three gait networks for the hexapod robot through CPG. Each gait network consists of 8 CPG oscillators used to control a specific gait of the robot. Then 6 CPG oscillators are used to form a gait selection network, and the corresponding gait network is selected according to the feedback information of the sensor, so as to achieve gait switching [21]. Haitao Yu *et al.* developed a two-layer single-leg controller based on CPG to realize the tripod gait of a six-legged robot. The high-level control is a set of CPG networks formed by the coupling of three VanderPol oscillators to adjust the phase relationship of the output signals. The low level control uses an auxiliary linear converter (LC) to convert CPG signals into joint trajectory. Finally, combine the single-leg controller with the finite state machine to make the hexapod robot have the ability to traverse obstacles and trenches autonomously [22]. Auke Jan Ijspeert *et al.* used the Kuramoto CPG network to develop Salamander, an amphibious robot. The Kuramoto CPG network consists of 20 CPG oscillators, which have the advantages of independently adjustable amplitude and phase of the oscillator. By adjusting the connection weight of the CPG network, achieve the switching of the motion mode from crawling to swimming [23], [24]. Alessandro Crespi, Auke Jan Ijspeert *et al.* also combined CPG with a finite state machine to develop a robotic fish, BoxyBot, which can swim and crawl. The finite state machine can not only switch between different gaits according to the feedback signals of the sensor, but also switch between swimming mode and crawling mode [25]. Munadi M *et al.* proposed a robotic salamander model based on CPG control, using three-dimensional animation to simulate the joint angle input generated by the CPG model, and realizing the linear walking of the robotic salamander [26]. Karakasiliotis K *et al.* proposed a method to construct a robotic salamander combined with high-speed radiography technology. The raw kinematic data extracted from the X-ray video is added to the joints of the robot to realize the basic motion behavior of the robotic salamander in water and on land, thus proving the movement ability of the robot salamander [27].

To improve the ability of underwater operations, this paper combines the advantages of bionic fish and foot robot, proposes a new underwater unmanned vehicle, the navigation and crawl underwater unmanned vehicle (NCUUV). It has the excellent maneuverability, concealment and propulsion efficiency of the bionic fish, and also has the good stability of the foot robot and the ability to adapt to the terrain. It can not only searches quickly by swimming, but also crawls and works on the seabed, and has good resistance to ocean currents.

The main intellectual contributions of this article are as follows: Firstly, a brand-new underwater vehicle—the navigation and crawl underwater unmanned vehicle (NCUUV) is proposed and designed, which combines the two modes of swimming and crawling. Secondly, the motion mode switching mechanism was designed to realize the switching of NCUUV between swimming and crawling. Finally, the CPG network reconstruction method is used to control the movement mode switching, and the free and smooth switching between swimming and crawling is completed.

The rest of the paper is organized as follows: Section 2 introduces the NCUUV's workflow and mechatronics design. Section 3 establishes the NCUUV's control framework of movement and motion mode switching. In Section 4, the effectiveness of the control method proposed in Section 3 is tested and verified. Finally, Section 5 gives conclusions and suggestions for future work.

II. MECHATRONIC DESIGN OF NCUUV

A. OVERALL DESIGN OF NCUUV

Traditional underwater robots have shortcomings such as small range of motion, susceptibility to ocean currents, and poor adaptability to terrain. Therefore, this paper proposes and designs a new type of underwater unmanned vehicle,

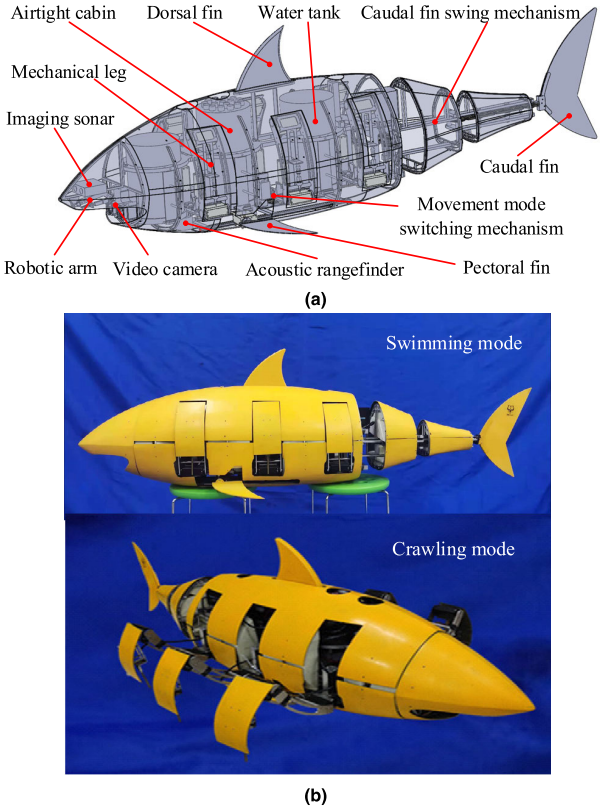

FIGURE 1. Navigation and crawl underwater unmanned vehicle (NCUUV) (a) 3-D model diagram (b) Engineering prototype.

the navigation and crawl underwater unmanned vehicle (NCUUV), as shown in Figure 1. It has two motion modes of swimming and crawling, and can carry different task loads according to different work requirements, such as the robot arm commonly used on ROV.

As can be seen from Figure 1, when swimming, NCUUV has the shape of a fish, and the caudal fin swing mechanism can simulate the motion of fish to provide power, and it has good propulsion efficiency. When crawling, the six bionic mechanical legs can adapt well to the rugged terrain of the seabed, improving the stability of NCUUV during crawling and working. By changing attack angle of the pectoral fin, NCUUV can be floated and dived. The water absorption and drainage of the water tank make NCUUV have the ability to vertically float and dive. The motion mode switching mechanism is responsible for switching between swimming and crawling of NCUUV.

The imaging sonar and underwater camera located on the head detect obstacles in front of the NCUUV and search for targets when swimming and crawling, respectively. The acoustic rangefinder located at the bottom of the NCUUV can detect the height from the seabed. NCUUV includes two airtight cabins, which are equipped with power and electronic circuits.

The workflow of NCUUV is as follows:

STEP 1: As shown in Figure 2, after entering the water, NCUUV searches for targets within a certain range by swimming mode.

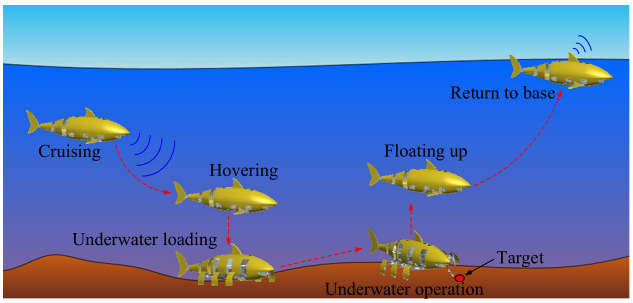

FIGURE 2. The workflow of NCUUV.

STEP 2: When the sonar detects the target, NCUUV swims towards the target. After swimming near the target, NCUUV hovers. Then the water tank absorbs water and NCUUV descends vertically. During the dive, NCUUV completed the switch from swimming to crawling, and then entered the crawling mode.

STEP 3: After NCUUV crawls to the target point, its body is supported by 6 mechanical legs, forming a working platform that can adjust position and posture. Finally, the robot arm is extended to complete the work on the target.

STEP 4: When the underwater operation is completed, the robot arm retracts and the NCUUV floats. Finally, the caudal fin starts to swing, and NCUUV returns to base.

B. DESIGN OF MOTION MODE SWITCHING MECHANISM

If 6 mechanical legs are installed directly on both sides of NCUUV, during crawling the swing of the mechanical legs will cause serious interference with the NCUUV's shell and pectoral fins. This will greatly weaken its crawling ability and even make it lose crawling ability. Therefore, how to combine the 6 mechanical legs with NCUUV is crucial.

As shown in Figure 3, in order to solve the above problem, this paper proposes a motion mode switching mechanism. It's a mechanical linkage mechanism, including 6 double slider mechanisms and 2 crank slider mechanisms, which are respectively used to drive the extension and retraction of 6 mechanical legs and 2 pectoral fins. The motor drives the master putter to move back and forth on the longitudinal slide through the rack and gear to provide power for the expansion and contraction of the double slider mechanisms and the crank slider mechanisms. The 6 mechanical legs and 2 pectoral fins are respectively fixed on the double slider mechanisms and the crank slider mechanisms to realize the contraction and expansion of the mechanical legs and pectoral fins. The motion mode switching mechanism is located at the bottom of NCUUV and is driven by only one motor, which greatly saves the internal space, reduces the control difficulty, and improves the reliability of motion mode switching.

The working process of the motion mode switching is shown in Figure 4. When NCUUV is in swimming mode, the motion mode switching mechanism is in the initial state, as shown in Figure 4 (a). When NCUUV switches the motion mode, the pectoral fins gradually contract to the bottom of NCUUV, at the same time, 6 mechanical legs extend from

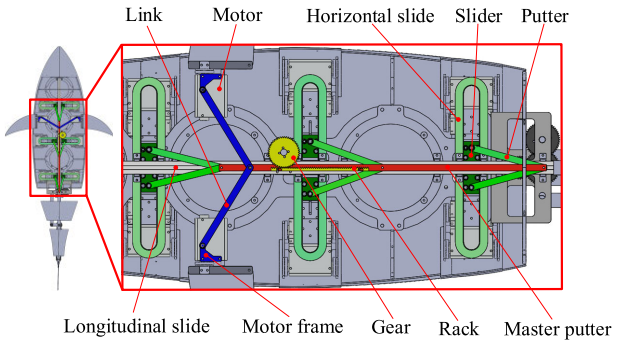

FIGURE 3. Motion mode switching mechanism.

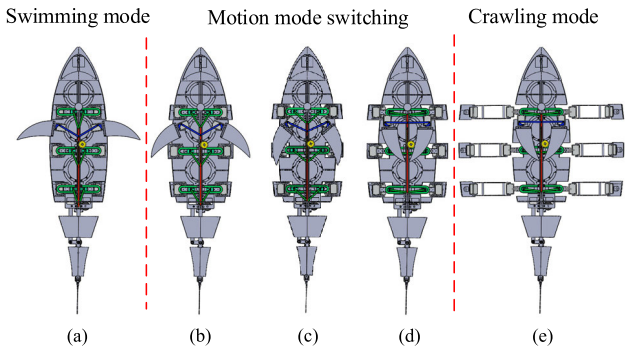

FIGURE 4. The working process of the motion mode switching.

both sides of NCUUV, as shown in Figure 4 (b)-(d). Finally, the mechanical legs are deployed and the NCUUV enters the crawling mode, as shown in Figure 4 (e). NCUUV from crawling mode switch to swimming is the reverse of the above process.

C. ELECTRONIC CIRCUIT DESIGN OF NCUUV

The hardware architecture of NCUUV is shown in the Figure 5, IMU can get the attitude, heading, 3D position and speed information of NCUUV. Imaging sonar and underwater camera detect the surrounding environment when NCUUV swims and crawls, respectively. Through the E180 wireless module and communication sonar, data interaction with the ground computer can be completed.

The acoustic rangefinder P30 and depth gauge feed the height and depth information of NCUUV back to the motion control computer Raspberry Pi 4 Model B, and the motion control computer adjusts the motion parameters to achieve autonomous movement.

In order to control the motor accurately and efficiently, a motor power supply board embedded with the STM32H743 chip is connected to the motion control computer for controlling the motor and information communication.

III. CPG-BASED MOTION CONTROL AND MODE SWITCHING

A. CPG MODEL FOR NCUUV

Commonly used CPG oscillators in actual projects include Matsuoka oscillator, Hopf oscillator, VanderPol oscillator,

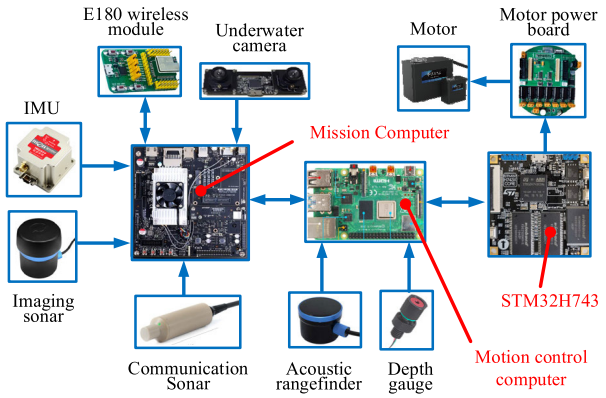

FIGURE 5. Hardware architecture of NCUUV.

TABLE 1. Technical specifications Of NCUUV.

Items	Characteristics
Dimension	1.74m×0.79m×0.62m
Weight	42.5 kg
Actuator	Servo (DS300, DS100, D30)
Controller	NVIDIA TW-TX-T300
	Raspberry Pi 4 Model B
	STM32H743
Control mode	Wireless or autonomous mode
Operation time	Approx. 1.5h
Joint motion range	hip joint: -13°~13°
	knee joint: 0°~30°
	ankle joint: 0°~10°
Mechanical leg stride length	0.26m
Underwater weight	Maximum weight: 460g

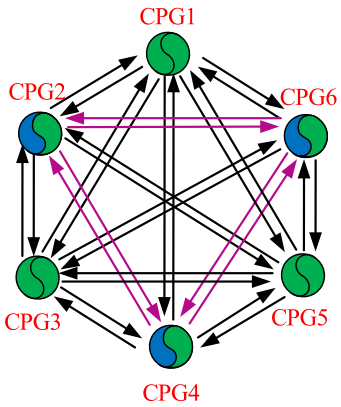

FIGURE 6. Topology diagram of composite CPG network.

Rayleigh oscillator and Hodgkin-Huxley oscillator. Among them, the Matsuoka oscillator has good biological characteristics and non-linearity, but has the disadvantages of many parameters, complicated structure, and difficult to adjust. VanderPol oscillator and Rayleigh oscillator models can generate human-like walking signals, which are mostly used for biped robot walking control. The Wilson-Cowan oscillator

has relatively few model parameters and a simple structure, but it exhibits asymmetry in a half-cycle, making it unsuitable as a controller for the bionic fish swinging tail motion. The Hopf oscillator can output a sine wave signal. Each parameter is independent and has a clear physical meaning and easy to adjust. So it is suitable for the motion control of bionic fish and hexapod robots. This provides the basic conditions for switching the motion mode, so this paper uses Hopf oscillator as the basic unit of CPG.

The mathematical model of the Hopf oscillator is as follows

$$\begin{cases} \dot{s}_i = \begin{bmatrix} \dot{x}_i & \dot{y}_i \end{bmatrix}^T = f_H(s_i) + k \sum_{j=1, j\neq i}^{n} \delta_{ij} T_{ij} \left(s_j - b_j\right)^T \\ f_H(s_i) = \begin{pmatrix} \alpha\left(A_i^2 - x_i^2 - y_i^2\right) & -\omega_i \\ \omega_i & \alpha\left(A_i^2 - x_i^2 - (y_i - b_i)^2\right) \end{pmatrix} s_i^T \\ R(\varphi_{ij}) = \begin{bmatrix} \cos\varphi_{ij} & -\sin\varphi_{ij} \\ \sin\varphi_{ij} & \cos\varphi_{ij} \end{bmatrix} \end{cases} \tag{1}$$

where, $i = 1, 2, \ldots, n$, n is the number of oscillators. A_i, ω_i, x_i, y_i represent the amplitude, frequency and state variables of the i-th oscillator, respectively. α is the convergence factor. δ_{ij} is the coupling weight, which determines the coupling strength between the oscillators. All of them form the coupling weight matrix W. A_i, x_j, y_j, and b_j are the amplitude, state variables and offset of the j-th oscillator. $T_{ij} = r_{ij}R(\varphi_{i,j})$, $r_{ij} = A_i/A_j$, $R(\varphi_{ij})$ is the two-dimensional rotation change matrix of φ_{ij} [28], $\varphi_{ij} = \varphi_i - \varphi_j$ is the phase difference between the i-th oscillator and the j-th oscillator. All the φ_{ij} form the phase matrix E. Since $\varphi_{ij} = -\varphi_{ji}$ and $\varphi_{ik} = \varphi_{ij} + \varphi_{jk}$ can easily get $T_{ij}T_{jk} = T_{ik}$ and $T_{ij}T_{ji} = I$, matrix T_{ij} contains information about the coupling amplitude and phase difference between oscillators.

When swimming, 3 Hopf oscillators are required to couple into a triangular network to control the two pectoral and caudal fins. When crawling, 6 oscillators are required to be coupled into a hexagonal network to control the swing of each mechanical leg. This paper uses a fully symmetrical hexagonal CPG network to control the movement of NCUUV, as shown in Figure10. The CPG network includes 6 oscillators. By adjusting the coupling relationship between the oscillators, the CPG network can switch freely between the triangular and hexagonal configurations, thereby realizing the control of swimming and crawling.

The crawling and swimming signals output by the CPG network are shown in Figure 7. It can be seen from the figure that the CPG network can generate a stable control signals in a short time, and the signals of the CPG network can achieve a smooth transition during the gait switching process.

B. PROOF OF THE STABILITY OF THE FULLY SYMMETRICAL HEXAGONAL CPG NETWORK

The dynamic characteristic of each oscillator in the fully symmetrical hexagonal network are as follows

$$\begin{aligned} \dot{s}_1 &= f_H(s_1) + k\left[\delta_{11}T_{11}(s_1 - b_1) + \delta_{12}T_{12}(s_2 - b_2)\right. \\ &\quad + \delta_{13}T_{13}(s_3 - b_3) \\ &\quad + \delta_{14}T_{14}(s_4 - b_4) + \delta_{15}T_{15}(s_5 - b_5) \\ &\quad \left. + \delta_{16}T_{16}(s_6 - b_6)\right] \\ \dot{s}_i &= f_H(s_i) + k\left[\delta_{i1}T_{i1}(s_1 - b_1) + \delta_{i2}T_{i2}(s_2 - b_2)\right. \\ &\quad + \delta_{i3}T_{i3}(s_3 - b_3) \\ &\quad \left. + \delta_{i4}T_{i4}(s_4 - b_4) + \delta_{i5}T_{i5}(s_5 - b_5) + \delta_{i6}T_{i6}(s_6 - b_6)\right] \\ \dot{s}_6 &= f_H(s_6) + k\left[\delta_{61}T_{61}(s_1 - b_1) + \delta_{62}T_{62}(s_2 - b_2)\right. \\ &\quad + \delta_{63}T_{63}(s_3 - b_3) \\ &\quad + \delta_{64}T_{64}(s_4 - b_4) + \delta_{65}T_{65}(s_5 - b_5) \\ &\quad \left. + \delta_{66}T_{66}(s_6 - b_6)\right] \end{aligned} \tag{2}$$

Equation (2) can be organized into matrix form

$$\dot{\widehat{s}} = \widehat{f}_H(\widehat{s}, \widehat{A}) - kG\widehat{s} \tag{3}$$

where, $\widehat{s} = [s_1, \cdots, s_6]^T$, $\widehat{f}_H(s) = [f_H(s_1), \cdots, f_H(s_6)]^T$, coupling matrix $G = D^{-1}WD$, $D = diag(T_{11}, T_{12}, \cdots, T_{16})$, W is the coupling weight matrix of the CPG network, a Laplacian matrix. $W_{ii} = \delta_{ii}I$, $W_{ij} = -\delta_{ij}I$, $\delta_{ii} = \sum_{j\neq i} \delta_{ij}$, where, $j \neq i$ and $i, j = 1, 2, \ldots, 6$. I is the second-order identity matrix, and the coupling matrix G is (4), as shown at the bottom of the next page.

We need to define a flow-invariant subspace of the CPG network, and the flow-invariant subspace satisfies the following conditions

$$\Delta_s = \left\{\widehat{s} \in R^{2N} \mid s_1 = T_{1i}s_i, \quad i = 2, 3, \cdots, 6\right\} \tag{5}$$

Transform the flow-invariant subspace in equation (3) into an equation about the first state vector, and obtain the

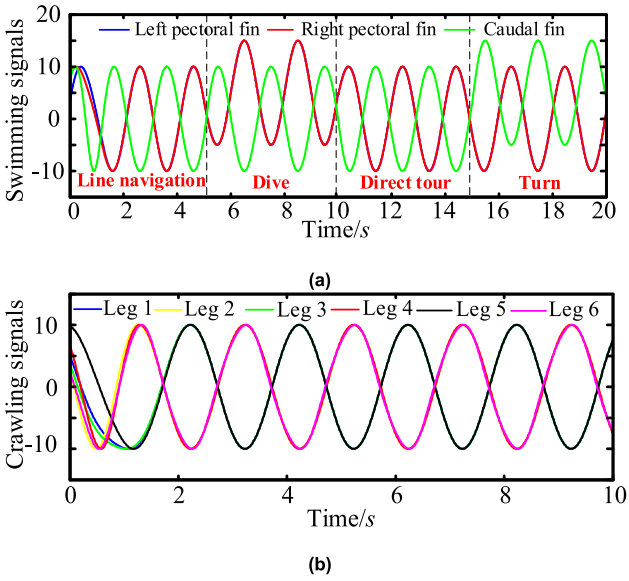

FIGURE 7. The output signals of CPG network (a) Swimming signals (b) Crawling signals.

equivalent flow-invariant subspace as

$$\Delta_{\widehat{s}} = \left\{ \widehat{s} \in R^{2N} \mid x_1 = x_2 = \cdots = x_6 \right\} \tag{6}$$

where, $\widehat{x} = [x_1, x_2, \cdots, x_6]^T$, $x_i = r_{1i} R(\varphi_{1i}) s_i$. Multiply by D to the left and use equation $\widehat{x} = D\widehat{s}$, we can get the equation of the CPG network in the new coordinate system as

$$\dot{\widehat{x}} = D\widehat{f}_H(\widehat{s}, \widehat{A}) - kL\widehat{x} \tag{7}$$

where, $\widehat{A} = [A_1, A_2, \cdots, A_6]$, because the limit cycle of the Hopf oscillator has symmetrical characteristics [29], $D\widehat{f}_H(\widehat{s}, \widehat{A}) = \widehat{f}_H\left(\widehat{x}, A_1\right)$ can be obtained, after equivalent transformation, the matrix equation of the CPG model is simplified.

For the sake of generality, the uneven value of the coupling weight in the CPG network should be considered, that is, discuss the stability of the CPG network when the coupling weight matrix W is unbalanced. In the fully symmetrical hexagonal CPG network as shown in Figure 6, any 3 or more oscillators can form a closed loop. For the same closed loop, whether it is in a clockwise or counterclockwise direction, the products of the connection weights are all equal. Therefore, according to the global exponential synchronization characteristics of the unbalanced CPG network [28], a new matrix V can be constructed to prove that when the coupling weights of the CPG network are not uniform, it does not affect the global exponential synchronization characteristics of the entire CPG network.

Introduce matrix $\Theta = diag(\Theta_1, \Theta_2, \cdots, \Theta_6)$ to balance equation (7)

$$\Theta_i = \begin{cases} I_2 & i = 1 \\ r_{1i}\sqrt{\prod_{j=1}^{i} \frac{\delta_{i-1,i}}{\delta_{i,i-1}}} I_2 & i = 2, 3, 4, 5, 6. \end{cases} \tag{8}$$

Let $\widehat{z} = \Theta\widehat{x}$, the following equation can be obtained

$$\dot{\widehat{z}} = \Theta\widehat{f}_H\left(\Theta^{-1}\widehat{z}, A_1\right) - k\Theta L\Theta^{-1}\widehat{z} \tag{9}$$

where, the new coupling matrix $\Theta L\Theta^{-1}$ is symmetric and positive semi-definite.

In the new coordinate system, the flow-invariant subspace is transformed into

$$\begin{aligned} \Delta_{\widehat{z}} = \Big\{ & \widehat{z} \in R^{2N} \mid \sqrt{\delta_{i,i+1}} R\left(\varphi_{i+1,i}\right) z_i \\ & = \sqrt{\delta_{i+1,i}} z_{i+1}, i \neq n, i \neq N \Big\} \end{aligned} \tag{10}$$

Using the constraint relationship in the equation of $\Delta_{\widehat{z}}$ to construct matrix V', its rows consist of the basis of $\Delta_{\widehat{z}}$, and orthogonalizing V' to obtain matrix V

$$V = \begin{bmatrix} \sqrt{\delta_{12}}R_{21} & -\sqrt{\delta_{21}}I & 0 \\ 0 & \sqrt{\delta_{23}}R_{32} & 0 \\ 0 & 0 & -\sqrt{\delta_{32}}I \\ 0 & 0 & \sqrt{\delta_{34}}R_{43} \\ 0 & 0 & 0 \\ 0 & 0 & 0 \\ 0 & 0 & 0 \\ -\sqrt{\delta_{43}}I & 0 & 0 \\ \sqrt{\delta_{45}}R_{54} & -\sqrt{\delta_{54}}I & 0 \\ 0 & \sqrt{\delta_{56}}R_{65} & -\sqrt{\delta_{65}}I \end{bmatrix} \tag{11}$$

According to the shrinkage theory [30], when the symmetric part of the generalized Jacobian matrix is always uniformly negative definite, that is, $VJ_SV^T < 0$, the system shown in Equation (7) converges globally and exponentially toward $\Delta_{\widehat{z}}$.

The Jacobian matrix of the system shown in Equation (7) is $J = \widehat{F} - \Theta L\Theta^{-1}$, where, $\widehat{F} = diag(F_1, F_2, \ldots, F_6)$, $F_i = \partial\left\{\Theta_i f\left(\Theta_i^{-1} z_i, A_1\right)\right\}/\partial z_i$. According to the amplitude characteristics of the Hopf oscillator, $f_H(rRx, A) = rRf_H(x, A/r)$, can get $F_i = \partial f_H(z_i, \Theta_i A_1)/\partial z$. $\widehat{F}_s$ is the symmetric part of $\widehat{F}$, $V\widehat{F}_SV^T$ has an upper bound and $V\widehat{F}_SV^T < \alpha I, \alpha$ is the convergence factor, all the convergence factors in the CPG network have the same value, and $\lambda_{max}(F_i) < \alpha$ can be obtained, where λ_{max} represents the largest eigenvector value of F_i.

Therefore, the sufficient condition of $VJ_SV^T < 0$ can be transformed into

$$\alpha < k\lambda_{min}\left(V\Theta L\Theta^{-1}V^T\right) \tag{12}$$

where, $\lambda_{min}(A)$ represents the minimum eigenvector value of matrix A. Because $\lambda_{min}\left(V\Theta L\Theta^{-1}V^T\right)$ is negatively definite, when the coupling gain k is large enough, $VJ_SV^T < 0$ holds. Therefore, $\widehat{z}$ can converge to $\Delta_{\widehat{z}}$ globally and at the same time converge to $\Delta_{\widehat{x}}$ globally. So far, the stability of the fully symmetrical hexagonal CPG network has been proved.

C. MOTION MODE SWITCHING METHOD BASED ON CPG NETWORK RECONSTRUCTION

The swimming of NCUUV is controlled by a fully symmetrical triangular CPG network, while the crawling is controlled by a fully symmetrical hexagonal CPG network. Therefore,

$$G = \begin{bmatrix} \delta_{11}I & -\delta_{12}T_{12} & -\delta_{13}T_{13} & -\delta_{14}T_{14} & -\delta_{15}T_{15} & -\delta_{16}T_{16} \\ -\delta_{21}T_{21} & \delta_{22}I & -\delta_{23}T_{23} & -\delta_{24}T_{24} & -\delta_{25}T_{25} & -\delta_{26}T_{26} \\ -\delta_{31}T_{31} & -\delta_{32}T_{32} & \delta_{33}I & -\delta_{34}T_{34} & -\delta_{35}T_{35} & -\delta_{36}T_{36} \\ -\delta_{41}T_{41} & -\delta_{42}T_{42} & -\delta_{43}T_{43} & \delta_{44}I & -\delta_{45}T_{45} & -\delta_{46}T_{46} \\ -\delta_{51}T_{51} & -\delta_{52}T_{52} & -\delta_{53}T_{53} & -\delta_{54}T_{54} & \delta_{55}I & -\delta_{56}T_{56} \\ -\delta_{61}T_{61} & -\delta_{62}T_{62} & -\delta_{63}T_{63} & -\delta_{64}T_{64} & -\delta_{65}T_{65} & \delta_{66}I \end{bmatrix} \tag{4}$$

the key to switching the motion mode is how to make the CPG network freely reconstruct between the two configurations of fully symmetrical hexagon and fully symmetrical triangle. The reconstruction of the CPG network is realized by establishing or disconnecting the coupling relationship between the oscillators, that is, the essence of the reconstruction of the CPG network is to transform the coupling weight matrix W of the CPG network.

Disconnect CPG1, CPG3 and CPG5 in the crawling CPG network from other oscillators can reconstruct the crawling CPG network into a swimming CPG network. The coupling weight matrix W and phase matrix E of the swimming CPG network and the crawling CPG network are shown in the Equation (13)-(16), respectively.

$$W_{swim\min g} = \begin{bmatrix} 0&0&0&0&0&0\\ 0&0&0&1&0&1\\ 0&0&0&0&0&0\\ 0&1&0&0&0&1\\ 0&0&0&0&0&0\\ 0&1&0&1&0&0 \end{bmatrix} \tag{13}$$

$$W_{crawling} = \begin{bmatrix} 0&1&1&1&1&1\\ 1&0&1&1&1&1\\ 1&1&0&1&1&1\\ 1&1&1&0&1&1\\ 1&1&1&1&0&1\\ 1&1&1&1&1&0 \end{bmatrix} \tag{14}$$

$$E_{swim\min g} = \begin{bmatrix} 0&0&0&0&0&0\\ 0&0&0&\pi&0&0\\ 0&0&0&0&0&0\\ 0&-\pi&0&0&0&-\pi\\ 0&0&0&0&0&0\\ 0&0&0&\pi&0&0 \end{bmatrix} \tag{15}$$

$$E_{crawling} = \begin{bmatrix} 0&-\pi&0&-\pi&0&-\pi\\ \pi&0&\pi&0&\pi&0\\ 0&-\pi&0&-\pi&0&-\pi\\ \pi&0&\pi&0&\pi&0\\ 0&-\pi&0&-\pi&0&-\pi\\ \pi&0&\pi&0&\pi&0 \end{bmatrix} \tag{16}$$

An acoustic rangefinder is installed at the bottom of the NCUUV to feed back the height h of the NCUUV from the seabed to the high-level controller. When the height h of NCUUV reaches the critical value h_1, the high-level controller transforms the coupling weight matrix W and phase matrix E in the CPG network, and then realizes the switching of the motion mode by reconstructing the CPG network. The relationship of the height h and the coupling weight matrix W and phase matrix E as shown in the Equation (17).

$$\begin{aligned} W &= \begin{cases} W_{swim\min g} & h > h_1 \\ W_{crawling} & h \le h_1 \end{cases} \\ E &= \begin{cases} E_{swim\min g} & h > h_1 \\ E_{crawling} & h \le h_1 \end{cases} \end{aligned} \tag{17}$$

The output signals of the CPG network before and after reconstruction is shown in the Figure 8. It can be seen from

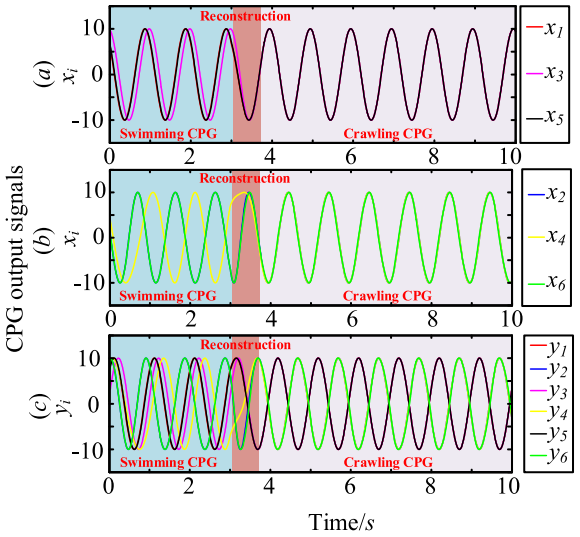

FIGURE 8. The output signals of the CPG network before and after reconstruction.

the Figure 8 (a) and Figure 8 (b) that before reconstruction, only the three oscillators of CPG2, CPG4 and CPG6 are coupled with each other to form a swimming CPG network, which can produce a stable phase difference within 1.5s. The output signals x_2, x_4 and x_6 can respectively control the NCUUV's left pectoral fin, caudal fin and right pectoral fin. There is no change in the phase of the output signal of the oscillators CPG1, CPG3 and CPG5 during the swimming process, so they vibrate independently and have no coupling relationship with other oscillators. When $t = 3s$, the CPG network starts to restructure. The 6 oscillators are coupled with each other to form a crawling CPG network. After 0.65s, the crawling CPG network produces a stable phase difference. At this time, the outputs of the 6 oscillators are divided into two groups, that is, x_1, x_3 and x_5 overlap each other, and x_2, x_4 and x_6 overlap each other. Two sets of signals control the two sets of mechanical legs in the tripod gait, respectively. It can be seen that the CPG network reconstruction method can well realize the NCUUV's motion mode switching.

The output signals of the CPG network need to be separated and amplified to control the swimming, crawling and motion mode switching of the NCUUV, respectively, so we mapped the output signals of the CPG network twice. The purpose of the first mapping is to separate the CPG signals that control the swimming from the numerous signals, and to set the duration of the motion mode switching. The purpose of the second mapping is to amplify the CPG signals into rotation angle signals that can control motors. The mapping functions of the first and second mapping are shown in Equation (18) and Equation (19).

$$\begin{cases} x_i^I = \begin{cases} 0 & (i = 1, 3, 5) \\ \lambda x_i & (i = 2, 4, 6) \end{cases}, \ h_1 < h \\ y_i^I = 0 \end{cases}$$
$$x_i^I = y_i^I = 0 \ (i = 1, 2, \cdots, 6), \ h_2 \le h \le h_1 \tag{18}$$
$$\begin{cases} x_i^I = x_i \\ y_i^I = y_i \end{cases} (i = 1, 2, \cdots, 6), h \le h_2$$

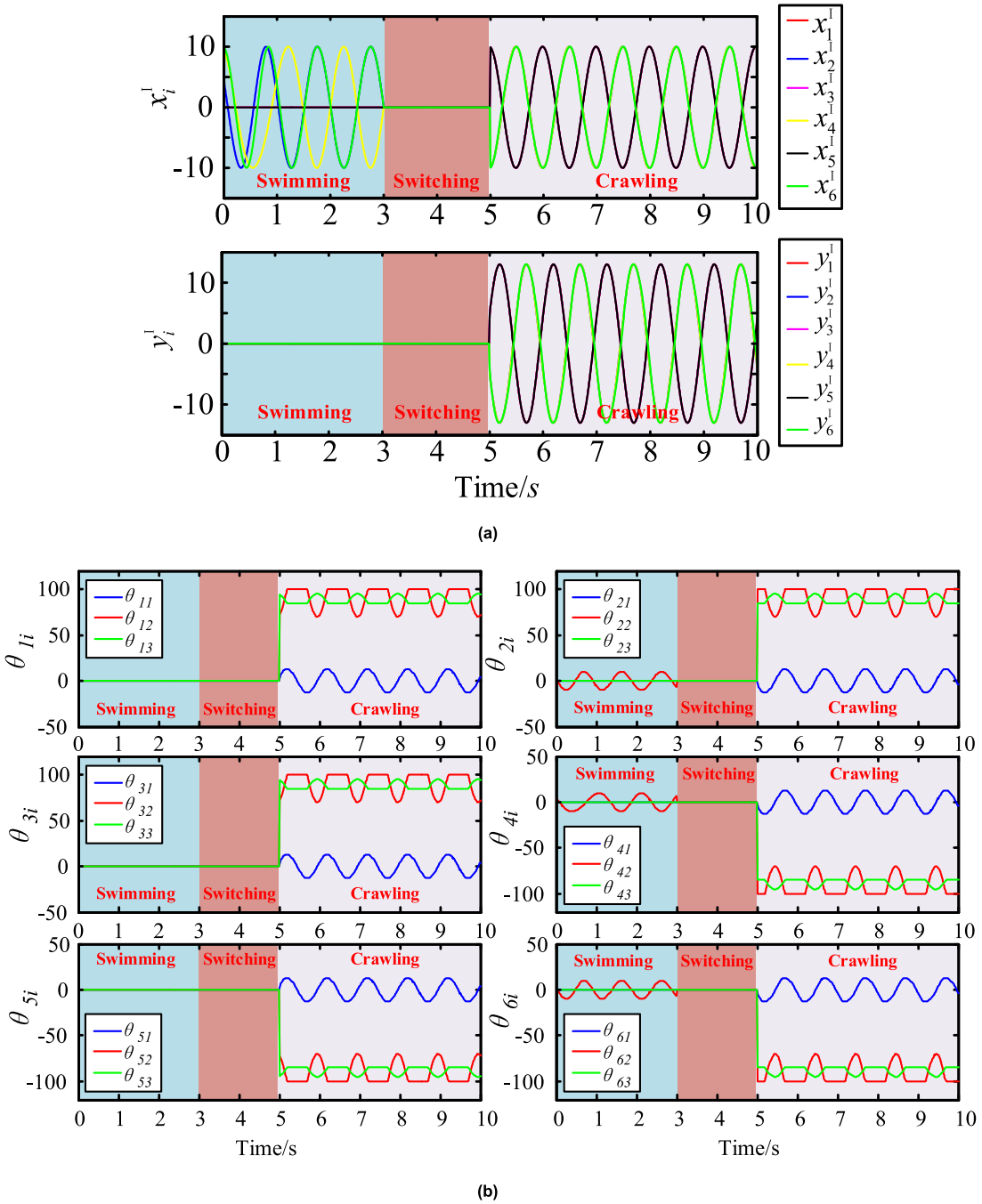

FIGURE 9. Output signals after mapping (a) The output signals of the first mapping (b) The output signals of the second mapping.

$$\begin{cases} \theta_{i1} = y_i^I \\ \theta_{i2} = \theta_{i3} = x_i^I \end{cases}, (i = 1, 2, \cdots, 6),\ h_2 < h$$

$$\begin{cases} \theta_{i1} = k_0 y_i^I \\ \theta_{i2} = \begin{cases} k_1 x_i^I + b_1 & (\dot{y}_i^I \geq 0) \\ k_2 x_i^I + b_2 & (\dot{y}_i^I < 0) \end{cases}, \ (i = 1, 2, \cdots, 6), h \leq h_2 \\ \theta_{i3} = \begin{cases} k_3 x_i^I + b_3 & (\dot{y}_i^I \geq 0) \\ k_4 x_i^I + b_4 & (\dot{y}_i^I < 0) \end{cases} \end{cases} \tag{19}$$

where, x_i^I and y_i^I represent the output signals after the first mapping. $\theta_{i1}, \theta_{i2}, \theta_{i3}$ represent the motor rotation angle signals generated after two mappings, $i = 1, 2, 3, \ldots, 6$. Adjusting the magnification factor $\lambda, k_0, k_1, k_2, k_3, k_4, b_1, b_2, b_3, b_4$ can change the output angle. h_1 and h_2 are the critical height values. When the height of NCUUV is higher than h_1, it is in the swimming mode. When the height is between h_1 and h_2, the motion mode is switched. When the height is lower than h_2, it is in the crawling mode.

Due to the limitation of the mechanical structure, and because the mechanical legs on the left and right sides are

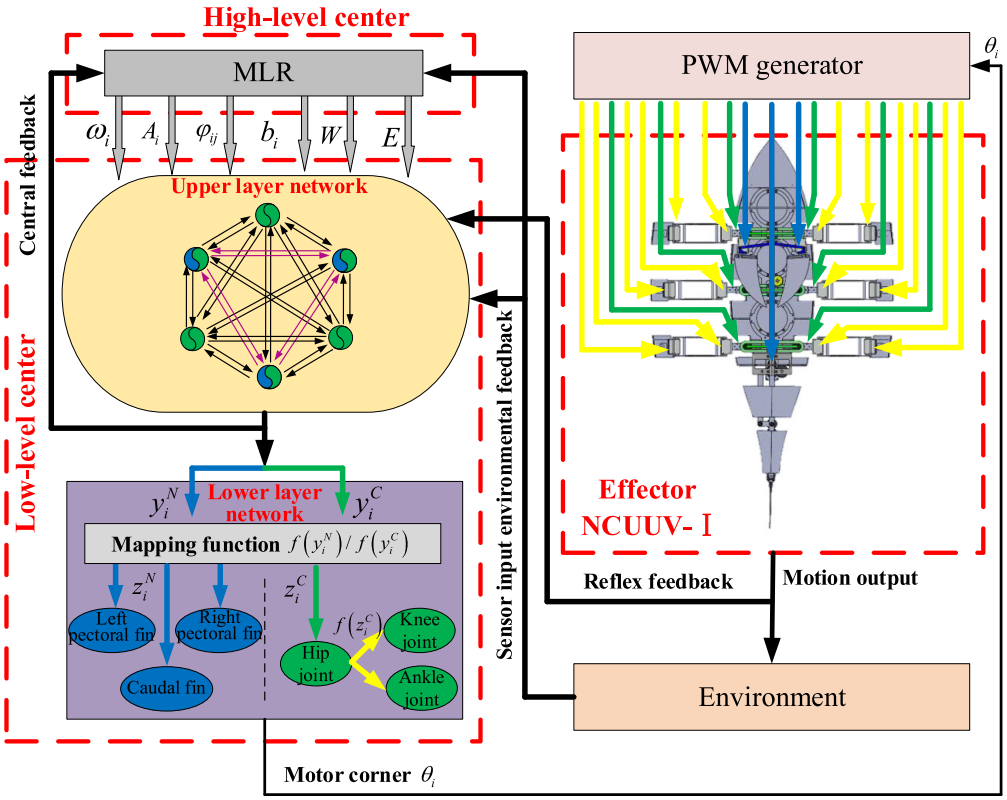

FIGURE 10. The CPG control principle diagram of NCUUV.

mirror images during the swing process, the angle values of the rotation are opposite to each other. take the amplification factor $\lambda = 1$, $k_0 = 1.3$, $k_1 = \pm 3$, $k_2 = 0$, $k_3 = \pm 1$, $k_4 = 0$, $b_1 = \mp 100$, $b_2 = \mp 100$, $b_3 = \pm 85$, $b_4 = \pm 85$, and get the output signals of the first mapping and the second mapping respectively as shown in Figure 9. It can be seen from Figure 9 (a) that after the first mapping, the controller only outputs three groups of signals x_2^I, x_4^I and x_6^I during the swimming process, and other signals are all 0. During the switching process, the output of all signals is 0 and the duration is $2s$. On the one hand, it provides time for the action of the motion mode switching mechanism, and on the other hand, it offsets the disordered signals generated during the reconstruction of the CPG network. When crawling, 6 sets of signals are released, and then the 6 mechanical legs are controlled, respectively. It can be seen from Figure 9 (b) that after the second mapping, during the swimming process, the three groups of motor angle signals θ_{22}, θ_{42} and θ_{62} output by the controller are sent to the motors of the left pectoral fin, caudal fin and right pectoral fin, and all other signals are 0. When crawling, the 6 groups of signals generated by the first mapping are mapped into 18 groups of motor angle signals, among them, θ_{i1}, θ_{i2}, θ_{i3} are the angle signals of hip joint, knee joint and ankle joint, respectively, $i = 1, 2, \ldots, 6$.

The CPG control principle diagram of NCUUV is shown in Figure 10. The control center of NCUUV includes high-level controller and low-level center. The high-level controller is the brainstem, which adjusts the CPG parameters of the low-level center according to the feedback signals of the sensor, so as to achieve the purpose of adjusting the output of the CPG network. The low-level center includes the upper-layer CPG network and the lower-layer mapping function. The CPG network generates corresponding output signals after being adjusted by the brainstem. These output signals are converted into rotation angle trajectories that control the pectoral fins, caudal fin, and mechanical legs through the mapping functions, and then the rotation angle trajectories send to PWM generator and brain stem separately. The PWM generator converts the rotation angle trajectories into PWM signals that can directly control the motor. Finally, the PWM signal is sent to each motor to control the rotation of the motor, thereby completing the motion control of NCUUV. The motion output signals of NCUUV and the environmental signals are feed back to the high-level controller and CPG network to further adjust the motion output of NCUUV.

IV. EXPERIMENT

In order to evaluate the effectiveness of the developed control method on NCUUV, on the basis of computer simulation, a more in-depth study on the performance of NCUUV's swimming, crawling and motion mode switching was carried out through experiments. As shown in the Figure 11,

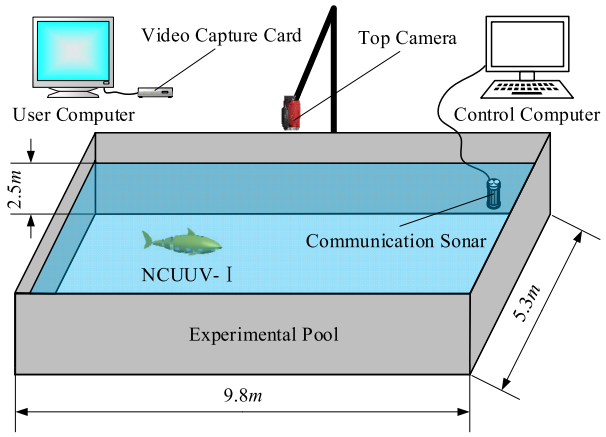

FIGURE 11. Schematic experimental platform.

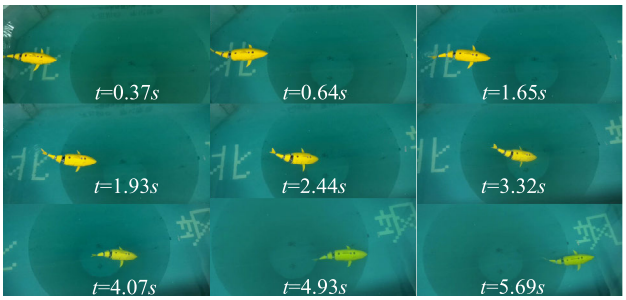

FIGURE 12. Swimming performance experiment.

an experimental system is designed to verify the movement performance of NCUUV. The experimental system includes environment, image capture module, communication module, data processing module and NCUUV. The pool is 5.3m wide, 9.8m long, and 2.5m depth. The system also includes a SONY HDR-CX680 top camera, a communication sonar, a user computer equipped with i5-7300HQ, 2.5GHz processor, 8GB DDR4 RAM and JOVISIONJVS-C301 video capture card and a control computer.

A. SWIMMING EXPERIMENT

The maximum rotation angles of the caudal and pectoral fins obtained by setting the mapping functions are 10°, when diving, the attack angle of the pectoral fin is 5°, and the swing frequency is 1.5Hz. The Figure 12 shows the swimming performance experiment of NCUUV.

Figure 12 shows that NCUUV swims very smoothly, and the swimming speed is 1.152m/s, that is, calculated according to the body length (BL), the speed is 0.662 BL/s, and the diving speed is 0.481m/s.

Then, through the control variable method, after many experiments, the effect of the joint rotation's amplitude A and frequency f on swimming and diving speed were tested respectively, and the results are shown in the Figure 13.

Experimental result shows that increasing the amplitude A and frequency f of the joint rotation can increase the forward

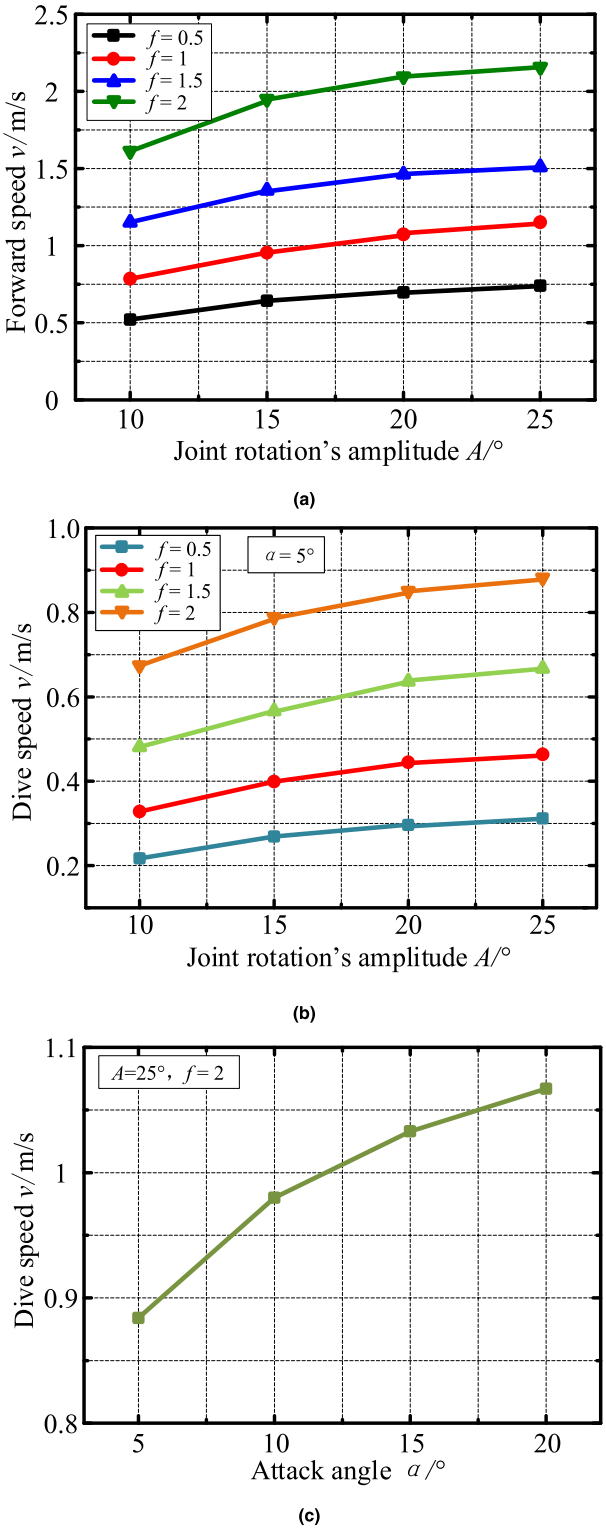

FIGURE 13. Swimming performance test results (a) The effect of the joint rotation's amplitude A and frequency f on forward speed (b) The effect of the joint rotation's amplitude A and frequency f on the dive speed (c) The effect of the attack angle α on the dive speed.

speed and the dive speed, and increasing the attack angle α can also increase the dive speed. When $A = 25°$ and $f = 2Hz$, the maximum forward speed is 2.116m/s, which is 1.216BL/s. When $A = 25°$, $f = 2Hz$, $\alpha = 20°$, the

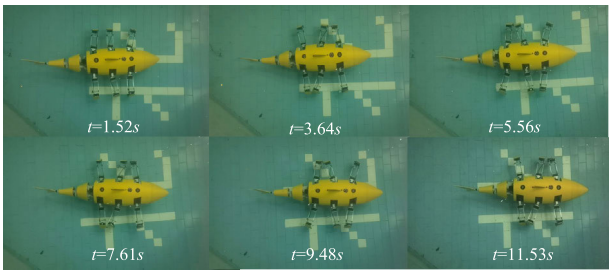

FIGURE 14. Crawling performance experiment.

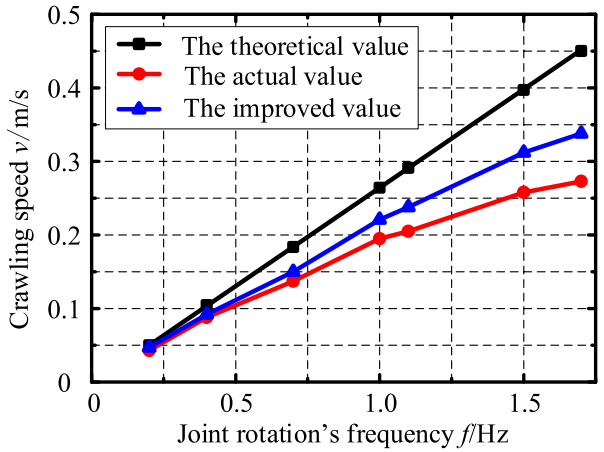

FIGURE 15. The effect of the joint rotation's frequency *f* on the crawling speed.

maximum diving speed is 1.324m/s. It can be seen from Figure 13 (a) and Figure 13 (b) that as the amplitude A of joint rotation increases, the acceleration of forward and downward decreases gradually. This is because as the amplitude A of joint rotation increases, the tail produces more thrust while also producing more resistance. Compared with this, increasing the frequency f of joint rotation can significantly increase the speed. It can be seen from Figure 13 (c) that increasing the attack angle α can also increase the dive speed, but the effect of increasing speed is no more significant than increasing the frequency f of joint rotation.

B. CRAWLING EXPERIMENT

By setting the mapping function, the swing amplitude of the hip joint of the NCUUV mechanical leg is 13°, and the frequency is $0.2Hz$. Figure 14 shows the crawling performance experiment process. It can be seen that the movement of each mechanical leg of NCUUV is very coordinated when crawling and there is no problem of mutual interference. The crawling speed is $0.05m/s$.

Through many experiments, the effect of the frequency f of joint rotation on the crawling speed has been tested, and the results are shown in the Figure 15.

The theoretical value of the crawling speed of NCUUV can be obtained by Equation (20).

$$v_{crawling} = Lf \tag{20}$$

where, L is the Mechanical leg stride length, $L = 0.26m$, f is the frequency of the mechanical leg swing.

The experimental result shows that increasing the frequency f of joint rotation can significantly increase the crawling speed of NCUUV. However, there is a significant gap between the actual value of the crawling speed and the theoretical value, and as the frequency increases, the difference between the actual value and the theoretical value becomes larger. This is because the ground of the experimental pool is relatively smooth. NCUUV has slipped during the crawling process, and as the crawling speed increases, the slipping phenomenon becomes more obvious. Therefore, when the frequency reaches $f = 1.7$, the crawling speed is only $0.27m/s$. In order to improve this problem, we have increased the water absorption of the tank from 220g to 460g to make NCUUV have greater gravity when crawling. The improved value is shown in the Figure 15, when the frequency reaches $f = 1.7$, the crawling speed is increased to $0.34m/s$. Although there is still a phenomenon of slipping, the crawling speed can be significantly increased by increasing the gravity, and the slippage problem can be improved.

C. MOTION MODE SWITCHING EXPERIMENT

After many experiments, we have determined the critical heights as follows: $h_1 = 1.5m$, $h_2 = 0.5m$. Then it is measured that it takes $2.44s$ for NCUUV to dive from depth h_1 to depth h_2, so the movement time of the motion mode switching mechanism is set to $2s$.

The experimental process of the motion mode switching is shown in Figure 16. Initially, NCUUV is in swimming mode. Then, NCUUV began to dive, it dives to the critical height $h_1 = 1.5m$ at $t = 6.35s$. At this time, the CPG network began to restructure, and transform from a fully symmetrical triangular network to a fully symmetrical hexagonal network. NCUUV stops swimming and the motion mode switching mechanism began to move forward. After $2s$, the 6 mechanical legs were fully extended from both sides of NCUUV, and the pectoral fins contracted to the abdomen. When NCUUV dives to the critical height $h_2 = 0.5m$ at $t = 9.43s$, the 6 mechanical legs unfold and enter the crawling mode, completing the switch from the swimming mode to the crawling mode.

When $t = 21.01s$, as the water tank drains and NCUUV starts to float. NCUUV floats up to the critical height h_2 =0.5m at $t = 25.27s$. At this time, the CPG network began to restructure, and transform from a fully symmetrical hexagonal network to a fully symmetrical triangular network. NCUUV stops crawling, after $2s$, the 6 mechanical legs retracted completely into the both sides of NCUUV, and the pectoral fins were expanded. When floating up to the critical height $h_1 = 1.5m$ at $t = 29.63s$, the caudal fin and pectoral fins begin to swing and enter the swimming mode, completing the switch from the crawling mode to the swimming mode.

Through the motion mode switching experiment, it can be seen that the motion mode switching mechanism can quickly

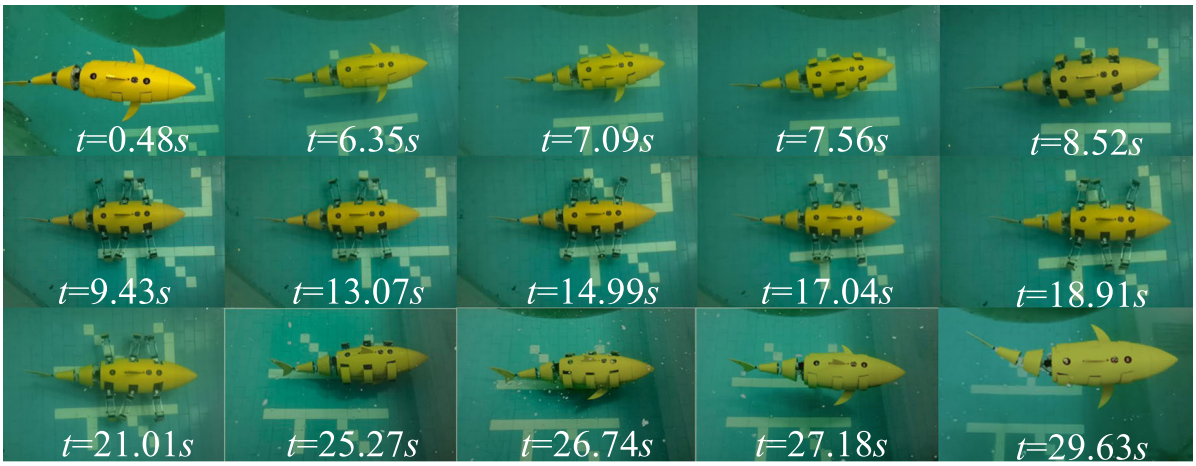

FIGURE 16. The experimental process of the motion mode switching.

and accurately complete the switching of the motion mode. The switching process is smooth and stable, and the retracting accuracy is very high. It solves the problem of mutual interference between mechanical legs, shell and pectoral fins during crawling, so that NCUUV has the basic conditions for free switching of motion modes. In addition, experiments have proved the effectiveness of the method of CPG network reconstruction proposed in this paper. This method can effectively solve the problem of free and smooth switching between the swimming and crawling modes of NCUUV. The high-level controller only adjusts the coupling weight matrix W and phase matrix E of the composite CPG network to realize the switching of the motion mode, so the control process is very simple and reliable.

V. CONCLUSION AND FUTURE WORK

In this work, we propose and design a navigation and crawl underwater unmanned vehicle (NCUUV) based on CPG control, which has two motion modes: swimming and crawling. In order to enable NCUUV to switch freely between the swimming and crawling modes, we designed a motion mode switching mechanism. And then by analyzing the characteristics of the CPG network, we propose a control method for motion mode switching based on CPG network reconstruction. Finally, through experiments, the depth critical values for controlling NCUUV to switch motion modes are determined. The experimental results show that by adjusting the coupling weight matrix W and phase matrix E of the CPG network, free and smooth switching of motion modes can be achieved. It also verifies the effectiveness of the motion mode switching mechanism. In addition, we also tested the swimming and crawling performance of NCUUV. We found that when swimming, increasing the amplitude and frequency of joint rotation can increase the forward speed and dive speed, and the effect of increasing the frequency is more significant. When crawling, as the frequency of joint rotation increases, the crawling speed also increases. At the same time, the phenomenon of mechanical legs slipping on the ground becomes more obvious. After adjusting the water absorption of the tank, the slipping phenomenon has been significantly improved.

In future work, we will adopt Newton-Euler method and Hamiltonian mechanics formula to establish the dynamic model of swimming and crawling, so as to improve the control accuracy of NCUUV and optimize the motion performance.

REFERENCES

[1] G. O. Koca, D. Korkmaz, Z. H. Akpolat, and M. Ay, "Implementations of the route planning scenarios for the autonomous robotic fish with the optimized propulsion mechanism.," *Measurement*, vol. 93, pp. 232–242, Nov. 2016, doi: 10.1016/j.measurement.2016.07.026.

[2] X. Niu and J. Xu, "Modeling, control and locomotion planning of an anguilliform robotic fish," *Unmanned Syst.*, vol. 2, no. 4, pp. 295–321, Oct. 2014, doi: 10.1142/S230138501440007X.

[3] M. Sfakiotakis, D. M. Lane, and J. B. C. Davies, "Review of fish swimming modes for aquatic locomotion," *IEEE J. Ocean. Eng.*, vol. 24, no. 2, pp. 237–252, Apr. 1999, doi: 10.1109/48.757275.

[4] J. Yu, L. Wen, and Z. Ren, "A survey on fabrication, control, and hydrodynamic function of biomimetic robotic fish," *Sci. China Technol. Sci.*, vol. 60, no. 9, pp. 1365–1380, Sep. 2017, doi: 10.1007/s11431-016-9065-x.

[5] B. Kwak and J. Bae, "Toward fast and efficient mobility in aquatic environment: A robot with compliant swimming appendages inspired by a water beetle.," *J. Bionic Eng.*, vol. 14, pp. 260–271, Jun. 2017, doi: 10.1016/S1672-6529(16)60396-7.

[6] T. G. Brown, "On the nature of the fundamental activity of the nervous centres; together with an analysis of the conditioning of rhythmic activity in progression, and a theory of the evolution of function in the nervous system," *J. Physiol.*, vol. 48, no. 1, pp. 18–46, Mar. 1914, doi: 10.1113/jphysiol.1914.sp001646.

[7] J. Yu, Z. Wu, M. Wang, and M. Tan, "CPG network optimization for a biomimetic robotic fish via PSO," *IEEE Trans. Neural Netw. Learn. Syst.*, vol. 27, no. 9, pp. 1962–1968, Sep. 2016, doi: 10.1109/TNNLS.2015.2459913.

[8] W. Wang, D. Gu, and G. Xie, "Autonomous optimization of swimming gait in a fish robot with multiple onboard sensors," *IEEE Trans. Syst., Man, Cybern. Syst.*, vol. 49, no. 5, pp. 891–903, May 2019.

[9] G. Zhong, L. Chen, Z. Jiao, J. Li, and H. Deng, "Locomotion control and gait planning of a novel hexapod robot using biomimetic neurons," *IEEE Trans. Control Syst. Technol.*, vol. 26, no. 2, pp. 624–636, Mar. 2018.

[10] C. Bal, G. Ozmen Koca, D. Korkmaz, Z. H. Akpolat, and M. Ay, "CPG-based autonomous swimming control for multi-tasks of a biomimetic robotic fish," *Ocean Eng.*, vol. 189, Oct. 2019, Art. no. 106334, doi: 10.1016/j.oceaneng.2019.106334.

[11] J. Yu, S. Chen, Z. Wu, X. Chen, and M. Wang, "Energy analysis of a CPG-controlled miniature robotic fish," *J. Bionic Eng.*, vol. 15, no. 2, pp. 260–269, Mar. 2018, doi: 10.1007/s42235-018-0020-1.

[12] M. Wang, H. Dong, X. Li, Y. Zhang, and J. Yu, "Control and optimization of a bionic robotic fish through a combination of CPG model and PSO," *Neurocomputing*, vol. 337, pp. 144–152, Apr. 2019, doi: 10.1016/j.neucom.2019.01.062.

[13] *CPG Network Optimization for a Biomimetic Robotic Fish Via PSO*, Biomimetics, Chin. Acad. Sci. Details Findings Biomimetics, Biotech Week, Beijing, China, 2016, doi: 10.1109/TNNLS.2015.2459913.

[14] M. Wang, Y. Zhang, H. Dong, and J. Yu, "Trajectory tracking control of a bionic robotic fish based on iterative learning," *Sci. China Inf. Sci.*, vol. 63, no. 7, pp. 505–518, Jul. 2020, doi: 10.1007/s11432-019-2760-5.

[15] Z. JiaQuan *et al.*, "Study of fuzzy control for biomimetic robot fish pose," *J. Guangxi Univ. Sci. Technol.*, vol. 28, no. 2, pp. 17–22, 2017.

[16] C. Niu, L. Zhang, S. Bi, and Y. Cai, "Development and depth control of a robotic fish mimicking cownose ray," in *Proc. IEEE Int. Conf. Robot. Biomimetics (ROBIO)*. Piscataway, NJ, USA: IEEE, Dec. 2012, pp. 814–818, doi: 10.1109/ROBIO.2012.6491068.

[17] K. Anh Hoang and T. Quan Vo, "A study on fuzzy based controllers design for depth control of a 3-joint carangiform fish robot," in *Proc. Int. Conf. Control, Autom. Inf. Sci. (ICCAIS)*. Piscataway, NJ, USA: IEEE, Nov. 2013, pp. 289–294, doi: 10.1109/iccais.2013.6720570.

[18] F. Shen, Z. Cao, C. Zhou, D. Xu, and N. Gu, "Depth control for robotic dolphin based on fuzzy PID control," *Int. J. Offshore Polar Eng.*, vol. 23, no. 3, pp. 166–171, 2013.

[19] Y. Zhu, T. Guo, Q. Liu, Q. Li, and R. Yan, "A study of arbitrary gait pattern generation for turning of a bio-inspired hexapod robot," *Robot. Auto. Syst.*, vol. 97, pp. 125–135, Nov. 2017, doi: 10.1016/j.robot.2017.08.012.

[20] J. Faigl and P. Cížek, "Adaptive locomotion control of hexapod walking robot for traversing rough terrains with position feedback only," *Robot. Auto. Syst.*, vol. 116, pp. 136–147, Jun. 2019, doi: 10.1016/j.robot.2019.03.008.

[21] D. Gutierrez-Galan, J. P. Dominguez-Morales, F. Perez-Peña, A. Jimenez-Fernandez, and A. Linares-Barranco, "Neuropod: A real-time neuromorphic spiking CPG applied to robotics," *Neurocomputing*, vol. 381, pp. 10–19, Mar. 2020, doi: 10.1016/j.neucom.2019.11.007.

[22] H. Yu, H. Gao, and Z. Deng, "Enhancing adaptability with local reactive behaviors for hexapod walking robot via sensory feedback integrated central pattern generator," *Robot. Auto. Syst.*, vol. 124, Feb. 2020, Art. no. 103401, doi: 10.1016/j.robot.2019.103401.

[23] A. J. Ijspeert, A. Crespi, D. Ryczko, and J.-M. Cabelguen, "From swimming to walking with a salamander robot driven by a spinal cord model," *Science*, vol. 315, no. 5817, pp. 1416–1420, Mar. 2007, doi: 10.1126/science.1138353.

[24] A. J. Ijspeert, "Central pattern generators for locomotion control in animals and robots: A review," *Neural Netw.*, vol. 21, no. 4, pp. 642–653, May 2008, doi: 10.1016/j.neunet.2008.03.014.

[25] A. Crespi, D. Lachat, A. Pasquier, and A. J. Ijspeert, "Controlling swimming and crawling in a fish robot using a central pattern generator," *Auto. Robots*, vol. 25, nos. 1–2, pp. 3–13, Aug. 2008.

[26] M. Munadi, M. Ariyanto, K. A. Pambudi, and J. D. Setiawan, "Development of 18 DOF salamander robot using CPG based locomotion for straight forward walk," *Int. Rev. Mech. Eng.*, vol. 13, no. 1, p. 70, Jan. 2019.

[27] K. Karakasiliotis, R. Thandiackal, K. Melo, T. Horvat, N. K. Mahabadi, S. Tsitkov, J. M. Cabelguen, and A. J. Ijspeert, "From cineradiography to biorobots: An approach for designing robots to emulate and study animal locomotion," *J. Roy. Soc. Interface*, vol. 13, no. 119, Jun. 2016, Art. no. 20151089, doi: 10.1098/rsif.2015.1089.

[28] K. Seo and J.-J.-E. Slotine, "Models for global synchronization in CPG-based locomotion," in *Proc. IEEE Int. Conf. Robot. Autom.*, Roma, Italy, Apr. 2007, pp. 281–286.

[29] S.-J. Chung and M. Dorothy, "Neurobiologically inspired control of engineered flapping flight," *J. Guid., Control, Dyn.*, vol. 33, no. 2, pp. 440–453, Mar. 2010.

[30] Q.-C. Pham and J.-J. Slotine, "Stable concurrent synchronization in dynamic system networks," *Neural Netw.*, vol. 20, no. 1, pp. 62–77, Jan. 2007.

ZHEPING YAN received the B.E. degree in nuclear power plants, the M.E. degree in special auxiliary devices and systems for marine and marine engineering, and the Ph.D. degree in control theory and control engineering from Harbin Engineering University, in 1994, 1997, and 2001, respectively. He is currently a Professor with the Institute of Marine Equipment and Control Technology, Harbin Engineering University. His research interests include underwater unmanned vehicle integration and testing, marine equipment automation and intelligent technology, and underwater robot technology.

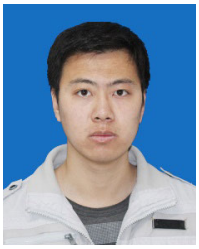

HAOYU YANG received the B.E. degree in mechanical engineering and automation from Shandong Jianzhu University, in 2016, and the M.E. degree in mechanical engineering from Harbin Engineering University, in 2019, where he is currently pursuing the Ph.D. degree in control science and engineering. His research interests include robotics and neural network control.

WEI ZHANG received the M.E. degree and the Ph.D. degree in control theory and control engineering from Harbin Engineering University, in 2004 and 2006, respectively. He is currently a Professor with the Institute of Marine Equipment and Control Technology, Harbin Engineering University. His research interests include overall design of underwater unmanned vehicle, mathematical modeling, intelligent control, and data fusion.

QINGSHUO GONG received the B.E. degree in mathematics and applied mathematics from the Henan University of Science and Technology, in 2019. He is currently pursuing the Ph.D. degree in control science and engineering with Harbin Engineering University. His research interests include robotic control and electrical control technology.

FANTAI LIN received the B.E. degree in measurement and control technology and instrumentation from North China Electric Power University, in 2019. He is currently pursuing the M.E. degree in control science and engineering with Harbin Engineering University. His research interests include robotics and neural network control.